Optik 125 (2014) 289–295

Contents lists available at ScienceDirect

Optik

journal homepage: www.elsevier.de/ijleo

Vehicle speed measurement based on gray constraint optical flow algorithm

Jinhui Lan [a,*], Jian Li [a,*], Guangda Hu [a], Bin Ran [b], Ling Wang [a]

[a] Department of Instrument Science and Technology, School of Automation and Electrical Engineering, University of Science and Technology Beijing, Beijing 100083, China
[b] Department of Civil and Environmental Engineering, School of Engineering, University of Wisconsin-Madison, Madison, WI 53706, USA

ARTICLE INFO

Article history:
Received 3 February 2013
Accepted 20 June 2013

Keywords:
Vehicle speed measurement
Gray constraint optical flow algorithm
Improved three-frame difference algorithm
Moving detection

ABSTRACT

Vehicle speed measurement (VSM) based on video images represents the development direction of speed measurement in the intelligent transportation systems (ITS). This paper presents a novel vehicle speed measurement method, which contains the improved three-frame difference algorithm and the proposed gray constraint optical flow algorithm. By the improved three-frame difference algorithm, the contour of moving vehicles can be detected exactly. Through the proposed gray constraint optical flow algorithm, the vehicle contour's optical flow value, which is the speed (pixels/s) of the vehicle in the image, can be computed accurately. Then, the velocity (km/h) of the vehicles is calculated by the optical flow value of the vehicle's contour and the corresponding ratio of the image pixels to the width of the road. The method can yield a better optical flow field by reducing the influence of changing lighting and shadow. Besides, it can reduce computation obviously, since it only calculates the moving target contour's optical flow value. Experimental comparisons between the method and other VSM methods show that the proposed approach has a satisfactory estimate of vehicle speed.

1. Introduction

Vehicle speed measurement plays an important role in the traffic information collection, and it is also a hot and difficult issue in ITS. At present, the vehicle speed measurement methods could be categorized into two types: (1) hardware-based methods and (2) software-based methods. The hardware-based methods consist of induction-coil loop speed measurement, laser speed measurement, radar speed measurement, etc. The software-based method is vehicle speed measurement by video images [1].

An induction-coil loop speed measurement method is a loop detector embedded into the ground. When the vehicles go across the loop, the loop's magnetic field changes, and the detector can calculate the vehicle speed. Since the induction-coil loop must be directly embedded in the lane, it will easily disrupt the road when it is installed or maintained. And the loop is also affected by the freezing, foundation subsidence and other factors. Moreover, the measurement accuracy will be greatly reduced when traffic slows [2,3]. For laser speed measurement, a laser detector is located above the roadway, it detects the moving object's distance and time for many times and then uses them to calculate the moving object's speed, which is based on the light waves speed measurement [4]. The laser detector can work day and night under different weather conditions, but extreme temperatures could yield performance loss in their functionalities [2,5]. Radar speed measurement adopts the Doppler radar effect. When the emission source or the receiver has relative motion, the received signal frequency will change. Radar speed measurements have a high demand on the angle of installation, which have limitations in the application [6].

For the vehicle speed measurement by video images, cameras are installed on the top of lane or placed alongside a roadway to shoot moving vehicles. The images captured by camera are analyzed by the image processing and pattern recognition algorithm, which are used to calculate the vehicle speed. The common methods used in the vehicle speed measurement by video images are corner detection, texture analysis, video tracking, and so on [7–12]. These methods can well find the matching location of the vehicle in the two consecutive image frames, but the large amount of computation cannot meet the requirements of real-time speed measurement. The method of virtual line can replace the real loop, but it is likely to create vehicle speed miscalculation because of the image frame acquisition period [13,14]. In addition, matching the different parts of vehicle in two consecutive images can affect the actual moving distance of the vehicle because of the size change of the bodies in the consecutive images [12,15,19].

* Corresponding authors at: School of Automation & Electrical Engineering, University of Science and Technology Beijing, Beijing 100083, China.
Tel.: +86 010 62334961.
E-mail addresses: ustblanjinhui@gmail.com, lanjh@ustb.edu.cn (J. Lan), gordonlj@163.com (J. Li).

0030-4026/$ – see front matter © 2013 Elsevier GmbH. All rights reserved.
http://dx.doi.org/10.1016/j.ijleo.2013.06.036

In order to overcome the shortcomings of various methods above, this paper states a novel vehicle speed measurement method based on improved three-frame difference algorithm and the gray constraint optical flow algorithm. Through the improved method, the contour of vehicles can be detected exactly. The optical flow value of the moving target contour can be computed precisely by the proposed gray constraint optical flow algorithm. The optical flow value is the speed (pixels/s) of the vehicle in the image. The method can reduce computation by only calculating the moving target contour's optical flow value. In the image, we draw the region of interest (ROI) and the speed of the vehicle in the ROI is computed. By the corresponding relation between the image pixels and the width of the road, the speed (km/h) of the moving target is calculated by the optical flow value.

The rest of this paper is organized as follows. In Section 2, vehicle speed measurement method proposed in the paper is described, where the improved three-frame difference method and the gray constraint optical flow method are introduced. Section 3 presents experimental results of our method and the results analysis. Finally, in Section 4, the conclusion on the experimental results is drawn.

2. Vehicle speed measurement method

The sensor used in the paper is a video camera installed on the top of lane. According to the camera, vehicles' information can be obtained. By the improved three-frame difference algorithm and the proposed gray constraint optical flow algorithm, the vehicles' motion parameters can be acquired. Then, the vehicle's velocity can be computed by the method.

2.1. Improved three-frame difference method

2.1.1. Interframe difference method

Interframe difference method is widely used in moving target detection by low computational complexity. In most cases, the performance is good. When target moves fast, the target's contour generated by two-frame video images produces overlap. So, the three-frame difference method is proposed [16].

The principle of the three-frame difference method is shown in (1)–(3):

$$p_1(x,y)=\begin{cases}255, & \text{if}|F_m(x,y)-F_{m-1}(x,y)|>T\\ 0, & \text{if}|F_m(x,y)-F_{m-1}(x,y)|\le T\end{cases} \tag{1}$$

$$p_2(x,y)=\begin{cases}255, & \text{if}|F_{m+1}(x,y)-F_m(x,y)|>T\\ 0, & \text{if}|F_{m+1}(x,y)-F_m(x,y)|\le T\end{cases} \tag{2}$$

$$\begin{aligned}p(x,y) &= p_1(x,y)\cap p_2(x,y)\\ &=\begin{cases}255, & \text{if}(p_1(x,y)=255\&\&p_2(x,y)=255)\\ 0, & \text{else}\end{cases}\end{aligned} \tag{3}$$

In (1) and (2), $F_{m-1}(x,y)$, $F_m(x,y)$ and $F_{m+1}(x,y)$ denote the gray value of the $m-1$ image frame, the m image frame and the $m+1$ image frame at the spatial pixel point (x,y). T is the threshold value. $p(x,y)$ is the gray value of spatial pixel point (x,y) of target image.

Although the three-frame difference method can get the moving target's contour, the detected contour is partly overlapped, which is compared to the real target's contour. The performance of the method is shown in Fig. 1. The green contour is the target contour, and the gray areas are overlap regions in the m frame contour.

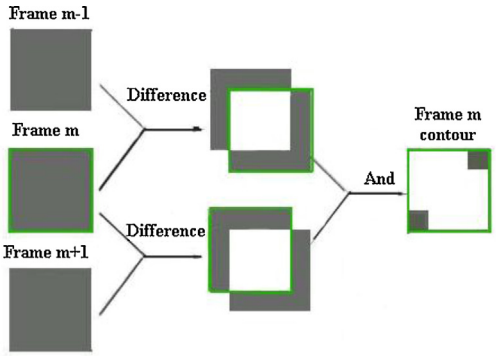

Fig. 1. Effect of three-frame difference's overlap.

2.1.2. Improved three-frame difference method

The result of the two-frame difference method produces overlap, and the three-frame difference algorithm also produces partly overlap. To eliminate the partly overlapped, this paper presents an improved three-frame difference algorithm. The algorithm can detect the target contour precisely, and can get contour information through the operation of the "difference", "dilate", "and" and "xor" in three consecutive frames.

Improved three-frame difference algorithm steps are as follows:

(1) The difference image p_1 is obtained by the first frame and the second image frames via the "difference" operation.

$$p_1(x,y)=\begin{cases}255, & \text{if}|F_m(x,y)-F_{m-1}(x,y)|>T\\ 0, & \text{if}|F_m(x,y)-F_{m-1}(x,y)|\le T\end{cases} \tag{4}$$

(2) The difference image p_2 is obtained by the second frame and the third image frames via the "difference" operation.

$$p_2(x,y)=\begin{cases}255, & \text{if}|F_{m+1}(x,y)-F_m(x,y)|>T\\ 0, & \text{if}|F_{m+1}(x,y)-F_m(x,y)|\le T\end{cases} \tag{5}$$

(3) The new image p_3 is derived from p_1 and p_2 via the "and" operation.

$$\begin{aligned}p_3(x,y) &= p_1(x,y)\cap p_2(x,y)\\ &=\begin{cases}255, & \text{if}(p_1(x,y)=255\&\&p_2(x,y)=255)\\ 0, & \text{else}\end{cases}\end{aligned} \tag{6}$$

(4) The new image p_6 is derived from the dilated images p_4 and p_5 via the "and" operation. SE is the 3×3 squared template, used to dilate the image.

$$\begin{aligned}&p_4(x,y)=p_1(x,y)\oplus SE\\ &p_5(x,y)=p_2(x,y)\oplus SE\\ &p_6(x,y)=p_4(x,y)\cap p_5(x,y)=\begin{cases}255, & \text{if}(p_4(x,y)=255\&\&p_5(x,y)=255)\\ 0, & \text{else}\end{cases}\end{aligned} \tag{7}$$

(5) The result image p is derived from p_3 and p_6 via the "xor" operation.

$$p(x,y)=p_3(x,y)\otimes p_6(x,y)=\begin{cases}255, & \text{if}(p_3(x,y)!=p_6(x,y))\\ 0, & \text{else}\end{cases} \tag{8}$$

It is known that global threshold T for image binarization could result in distortion in a real image whose intensities vary gradually

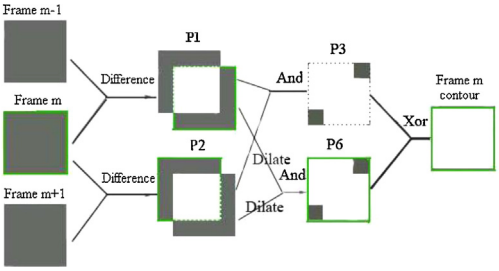

Fig. 2. Effect of improved three-frame difference.

due to illumination. Therefore, we adopt the local adaptive threshold segmentation method to extract the target from background. The global adaptive threshold T is used to do the initial segmentation. The thresholding value T for the whole image is determined by the difference between the mean and standard deviations of the whole image.

Thresholding value T = mean − std.

The effect of improved three-frame difference algorithm is shown in Fig. 2. From the figure, the precision contour of target can be obtained by the method. So, the algorithm has a better result than three-frame difference algorithm. In particular, when the velocity of the moving target is faster, the effect is more obvious.

To illustrate the superior performance of the improved method, experiments are done by the three kinds of frame difference method. Fig. 3 shows the original image, and they are 640 × 480 pixels. The computed threshold value T is 102 from the images. Fig. 4(a) shows the performance of two-frame difference method, Fig. 4(b) shows the performance of three-frame difference method and Fig. 4(c) shows the performance of the method proposed in this paper.

From Fig. 4, it is easy to make the conclusion as follows: Two-frame difference method produces overlap obviously. Three-frame difference method produces overlap at the corners of the car's contour. The contour obtained by using this paper proposed algorithm is precise, which is shown in Fig. 4(c). Also, the number of the white edge points is 4530 in Fig. 4(a), 2573 in Fig. 4(b) and 2061 in Fig. 4(c), respectively. So, the improved three-frame difference method has good performance.

For multi-target motion detection, the proposed algorithm can be used as the initial partition, and then use the gray constraint optical flow method to compute the moving targets' velocity.

2.2. Basic equation of optical flow and the improved algorithm

The change of the gray value expressed by optical flow field can be used to observe the information of moving target in the image. It contains the information of the image point's instantaneous velocity vector of the target. According to the velocity vector, the velocity of the target can be calculated.

2.2.1. Basic equation of optical flow

Optical flow is proposed by Gibson at first, and it is the moving velocity of target in the gray mode. The calculation of moving target's optical flow field is based on two assumptions: (1) the gray value of a moving object is unchanged in a very short time; (2) each pixel of the target has the same speed because of the target's rigid properties [17].

Suppose that the point P in the image coordinates at (x,y) moves to $(x+dx,\ y+dy)$ after dt. The gray value is $I(x,y,t)$ at (x,y) and $I(x+dx, y+dy, t+dt)$ at $(x+dx, y+dy)$. As dt is short, the gray value is unchanged by the assumption, and it is shown in (9). Also, (9) is called the basic optical flow equation.

$$I(x+dx, y+dy, t+dt) = I(x, y, t) \tag{9}$$

The left side of (9) is expanded using Taylor's formula, and is shown as follows.

$$I(x+dx, y+dy, t+dt) = I(x, y, t) + \frac{\partial I}{\partial x}\frac{dx}{dt} + \frac{\partial I}{\partial y}\frac{dy}{dt} + \frac{\partial I}{\partial t}\frac{dt}{dt} + o(\delta t^2) \tag{10}$$

After simplification and ellipsis the quadratic term, the basic optical flow equation (9) is simplified to (11).

$$\frac{\partial I}{\partial x}\frac{dx}{dt} + \frac{\partial I}{\partial y}\frac{dy}{dt} + \frac{\partial I}{dt}\frac{dt}{dt} = 0 \tag{11}$$

$u = dx/dt$ and $v = dy/dt$ are the moving speed of the pixel at the image spatial pixel point (x, y) in horizontal and vertical directions.

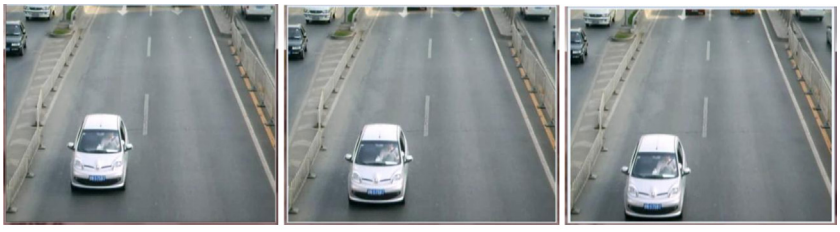

(a) (b) (c)

Fig. 3. The original image: (a) the 529th image, (b) the 530th image, and (c) the 531st image.

(a) (b) (c)

Fig. 4. Effect of difference methods: (a) two-frame difference method image, (b) three-frame difference method image, and (c) improved three-frame difference method image.

Also, (u, v) is called for the optical flow field. The basic optical flow equation (11) can be expressed as (12) [18,19]

$$(I_x, I_y)(u, v)^T + I_t = 0 \tag{12}$$

where $I_x = \partial I/\partial x$, $I_y = \partial I/\partial y$, $I_t = \partial I/\partial t$.

2.2.2. Gray constraint optical flow algorithm

In practical application, the assumption that the gray value is unchanged in a very short time in the optical flow field cannot be met for the reasons of block, multi-source, transparency and so on. According to the generalized dynamic image mode (GDIM), the gray value is not constant, but changed. So, the basic equation of optical flow (9) and (11) does not hold, we propose the gray constraint optical flow equation, and it can be expressed as follows:

$$I(r + \Delta r) = M(r)I(r) + C(r) \tag{13}$$

where $I(r) = I(x,y,t)$, $M(r) = 1 + \Delta m(r)$, $\Delta m(r)$ is the deviation coefficient. $C(r)$ is interference.

The gray constraint optical flow equation is shown as follows (13):

$$I(r + \Delta r) = I(r) + \Delta m(r)I(r) + C(r) \tag{14}$$

If $\Delta m(r) = C(r) = 0$, (14) meets the gray value unchanged assumption of the basic optical flow equation, and it is the same with (9). In practical application, the gray constraint optical flow equation (13) is suited for the actual situation. Also, the gray constraint optical flow error is shown as below:

$$\Delta I = I(r + \Delta r) - I(r) = \Delta m(r)I(r) + C(r) = I_x u + I_y v + I_t \tag{15}$$

After deformation, (15) is expressed as follows:

$$\Delta I = \Delta g + I_t \tag{16}$$

where $\Delta g = (I_x u + I_y v)$.

In (16), Δg is the geometric component (the speed of moving objects), ΔI is the illumination component, and the ratio $Y = \Delta g/\Delta I$ can be used as the parameter of relative strength between Δg and ΔI. If the ratio is large, the velocity component estimated is quite accurate. On the contrary, the estimated speed is not accurate, and the affection of light is large. The ratio is significant for the estimation of the motion parameters and the structural parameters. Therefore, the value of Y can be used to constrain the optical flow field distribution, which can make the optical flow algorithm perform well under a variety of challenging light, traffic condition, and so on.

Since LK (Lucas–Kanade) method may not perform well in dense flow field, HS (Horn and Schunck) method can detect minor motion of objects and provide a 100% flow field. Thus, we focus on HS method for optical flow field computation in our research [19].

2.2.3. Motion constraint equations of Horn and Schunck

To meet the assumptions that the optical flow field caused by the same moving object should be smooth, Horn and Schunck propose the smoothness constraint condition, which varies by the integral of the velocity components square. The smoothness constraint error is represented by (17). It calls for (17) to be as small as possible for the purpose of the smoothness [17,19].

$$E_s = \iint \left[\left(\frac{\partial u}{\partial x}\right)^2 + \left(\frac{\partial u}{\partial y}\right)^2 + \left(\frac{\partial v}{\partial x}\right)^2 + \left(\frac{\partial v}{\partial y}\right)^2 \right] dxdy \tag{17}$$

On the other hand, the assumption that the gray value is unchanged in the optical flow field cannot be met for many reasons. So, it requires that the proposed gray constraint optical flow error (15) is as small as possible, and it is expressed as (18).

$$E_c = \int (\Delta I)^2 dxdy = \int (I_x u + I_y v + I_t)^2 \, dx \, dy \tag{18}$$

To meet the proposed gray constraint optical flow error and the smoothness constraint error, Eq. (19) is set to find the solution of the optical flow (u,v).

$$E = \iint (E_c + \lambda E_s) \, dx \, dy = \iint \left\{ (I_x u + I_y v + I_t)^2 + \lambda \left[\left(\frac{\partial u}{\partial x}\right)^2 + \left(\frac{\partial u}{\partial y}\right)^2 + \left(\frac{\partial v}{\partial x}\right)^2 + \left(\frac{\partial v}{\partial y}\right)^2 \right] \right\} dx \, dy = \min \tag{19}$$

λ is the parameter that determines the weight between the two errors (the error of deviation from the smoothness E_s and the optical flow error E_c). When the image gray value of the measurement is accurate, and the λ can be made larger, which gives greater emphasis on E_c. Conversely, if the image contains a lot of noise, λ is a desirable small (less than 1) value.

The corresponding Euler equation of (19) is expressed as follows:

$$\begin{aligned} I_x(I_x u^{(n+1)} + I_y v^{(n+1)} + I_t) &= -\lambda \nabla^2 u \\ I_y(I_x u^{(n+1)} + I_y v^{(n+1)} + I_t) &= -\lambda \nabla^2 v \end{aligned} \tag{20}$$

where ∇^2 is the Laplacian operator and n denotes the number of iteration. Suppose $\nabla^2 u = u^{(n+1)} - \bar{u}^{(n)}$, $\nabla^2 v = v^{(n+1)} - \bar{v}^{(n)}$. $\bar{u}$, $\bar{v}$ denote the average optical flow value of u, v, what can be derived from the local smoothing template of the images. The size of the template depends on the requirements of the image. Considering only the computation, the size of the template is 3×3, the result in (20) can be written as follows:

$$\begin{aligned} (I_x^2 + \lambda)u^{(n+1)} + I_x I_y v^{(n+1)} &= \lambda \bar{u}^{(n)} - I_x I_t \\ (I_y^2 + \lambda)v^{(n+1)} + I_x I_y u^{(n+1)} &= \lambda \bar{v}^{(n)} - I_y I_t \end{aligned} \tag{21}$$

Therefore, a natural iteration method solution of optical flow is obtained by (21).

$$\begin{aligned} u^{(n+1)} &= \bar{u}^{(n)} - \frac{I_x(I_x \bar{u}^{(n)} + I_y \bar{v}^{(n)} + I_t)}{\lambda + I_x^2 + I_y^2} \\ v^{(n+1)} &= \bar{v}^{(n)} - \frac{I_y(I_x \bar{u}^{(n)} + I_y \bar{v}^{(n)} + I_t)}{\lambda + I_x^2 + I_y^2} \end{aligned} \tag{22}$$

where n denotes the number of iteration, u^0 and v^0 denote the initial value of the optical flow, which take zero. When the results of the distance between two iterations are less than the threshold, iterations are terminated. The optical flow is $(u^{(n+1)}, v^{(n+1)})$. According to the value of $u^{(n+1)}$ and $v^{(n+1)}$, the velocity in the pixel P is expressed as (23), and also the pixel P's direction is expresses as (24).

$$f_p = \sqrt{u^{(n+1)^2} + v^{(n+1)^2}} \tag{23}$$

$$\theta = \arctan \frac{v^{(n+1)}}{u^{(n+1)}} \tag{24}$$

In order to show the effect of the proposed gray constraint optical flow algorithm, tests have been done by video image. The gray constraint optical flow algorithm and the basic optical flow algorithm are compared. In the tests, the moving target's contour is obtained by the improved three-frame difference method. The ratio Y is set to 1, and the parameter λ is 1. The images are shown in

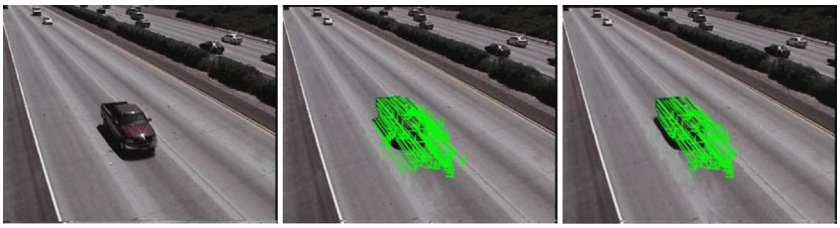

(a) (b) (c)

Fig. 5. (a) The original image, (b) effect of the improved three-frame and the basic optical flow algorithm, and (c) effect of the improved three-frame and the proposed constraint optical flow algorithm.

Fig. 5(b) and (c). In the figures, when the optical flow value f_p is bigger than the threshold value, the optical flow field is shown.

From the figures, it is shown that the gray constraint algorithm is well-distributed in the optical flow field and can perform well under a variety of challenging lighting and shadow. So, the improved algorithm can work better than the basic optical flow algorithm.

2.3. Vehicle speed measurement

In the vehicle speed measurement system, cameras are the majority of vision devices used. According to that whether the camera need to calibrate by manual, the vision-based VSM systems can be classified into two main models: (1) the calibrated camera model [20,21] [our system] and (2) the uncalibrated camera model [22–25].

In the calibrated camera model, the appropriate positions of vehicles are estimated by the geometric parameters of focal length, installation angle and installation height. Fig. 6 shows the installation schematic diagram [1].

This paper considers the issue that the camera is tilted downward and mounted at a fixed location on a bridge crossing the street. In the image, not all image is regions of interest. Adjusting the focal length, installation angle and installation height of the camera, we delineated a region of interest (ROI) from the image. As shown in Fig. 7, the area enclosed by green line is the detection area. In the vertical direction, the intersection point between the two white lines of the double-lane and the edge of the image is the middle point of the ROI, and the region can contain the whole contour of the car.

When the perspective effect is not considered, the width of road in the ROI is equal to the image width (horizontal direction). Suppose the image extracted from video is 640 × 480 pixels, and 7.5 m is the standard width of double-lane national road. So the ratio of

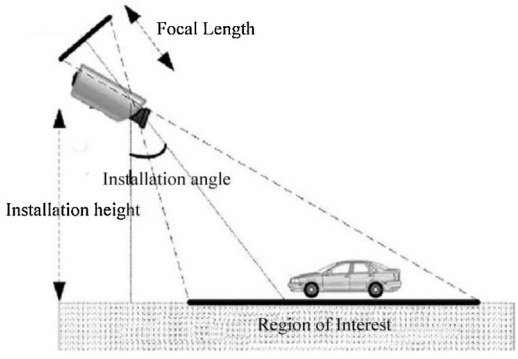

Fig. 6. Installed schematic diagram.

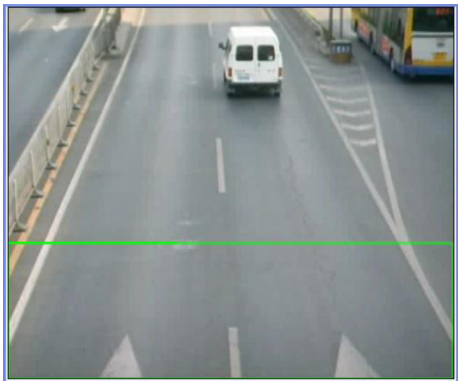

Fig. 7. Region of interest.

the pixels in the image and the width of the road are expressed as below:

$$k = \frac{7.5\ \text{m}}{640\ \text{pixels}} = 7.5/640\ \ (\text{m/pixel}) \tag{25}$$

In the ROI, all detected moving targets are marked by the improved three-frame difference method, and the speed of all points in every moving block are calculated, then the speed of the target is computed by the average speed of all points in the target. The speed of the target is shown as (26).

$$f_{avr} = \frac{1}{n}\sum_{p=1}^{n} f_p \tag{26}$$

where n denotes the number of points in the moving target obtained by the improved three-frame difference algorithm, f_p denotes the optical flow geometry value of the point of target. f_{avr} denotes the optical flow geometry value of the block. According to the geometric value f_p of the moving block and the ratio k between the image pixels and the width of the road, the vehicle velocity is given as follows:

$$V = f_{avr} \times k \tag{27}$$

3. Experimental results and analysis

This paper presents a vehicle speed measurement method based on the improved three-frame difference algorithm and the proposed gray constraint optical flow algorithm. The method was carried out by VC++6.0 with OpenCV, and ran in MS Windows XP environment. Several tests were performed to validate the proposed method. All tests were done on a PC with 1.9 GHz Celeron processor and 1024 MB RAM. The vehicles, move toward or away from the camera in the two-lane, are shot by the SONY HDR-XR260E camera tilted downward and mounted at a fixed location on a bridge crossing the target street at 6 m high. The video used in the test has 30 frames rate and the resolution is 640 × 480 pixels.

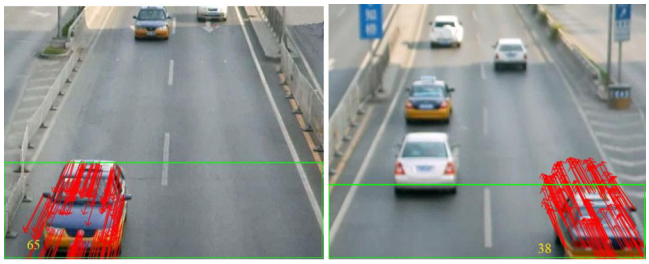

(a) (b)

Fig. 8. A vehicle in the ROI of the two-lane: (a) a vehicle move toward the camera and (b) a vehicle move away from the camera.

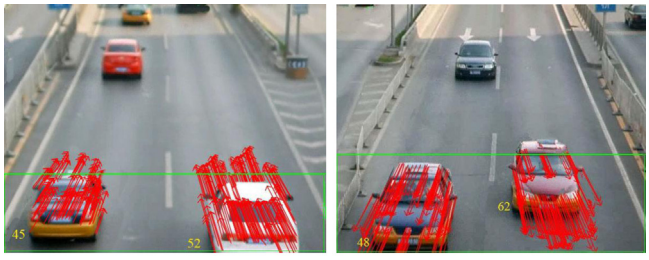

(a) (b)

Fig. 9. Two vehicles in the ROI of the two-lane: (a) two vehicles move toward the camera and (b) two vehicles move away from the camera.

3.1. Vehicle speed measurement by the proposed method

For evaluating the performance of the proposed method, vehicles are used to do experiments. Fig. 8 shows the performance of a vehicle's speed measurement in the double-lane in two different directions, Fig. 9 shows two vehicles' speed measurement effect. Red arrows denote the velocity of vehicle. 1000 cars' velocity from two different directions is measured. The experimental results are compared with the velocity measured by radar. We estimate the vehicle's velocity V_{opt} by the method and measure the velocity V_{radar} by radar at the same time. The error is computed by the equation $\left|V_{radar} - V_{opt}\right| / V_{radar}$. The average error is statistics when the V_{radar} is in the velocity range, and results are expressed in Tables 1 and 2.

Table 1
Vehicle move toward the camera.

Velocity range/km/h	The number of vehicle	Average error (%)
0–20	85	2.5
20–40	110	1.5
40–60	139	0.9
60–80	302	0.8
80–100	272	1.0
100–120	76	1.1
120–140	12	1.3
Above 140	4	1.5

Table 2
Vehicles move away from the camera.

Velocity range/km/h	The number of vehicle	Average error (%)
0–20	79	1.3
20–40	123	1.1
40–60	164	0.9
60–80	295	0.8
80–100	254	0.9
100–120	67	1.2
120–140	15	1.4
Above 140	3	1.7

Table 3
Average errors in different velocity range by the methods (%).

Velocity range/km/h	Method			
	Paper [1]'s method	Paper [2]'s method		Our method
		IFD	BS	
0–20		4.2	5.6	1.9
20–40	0.68	4.1	5.3	1.3
40–60	9.7	3.5	3.0	0.9
60–80	5.6	2.2	1.1	0.9
80–100	6.6	1.5	1.5	1.0
100–120	3.7	0.7	2.3	1.2
120–140		1.9	1.2	1.4
Above 140				1.6

Experiments show that the method can measure the vehicle speed accurate and real-time. Figs. 8 and 9 show the performance of the proposed method. The test results (see Tables 1 and 2) show that the error range of the speed measurement is relatively small. But when the velocity of vehicles is too fast or too small, the error of the results is large. When the vehicle is completely in ROI, the performance of the method is the best.

From the test results (see Tables 1 and 2), they show that the rate of error increases when the velocity is relatively large or small, that is because the actual ratio of the pixels in the image and the width of road are deviated from the ratio K.

According to the proposed method, the processing time of each frame is 25 ms, which is less then 45 ms by the basic optical flow method. Also it can meet the requirement of the real-time.

3.2. Compared with other VSM methods

In order to show the performance of the described method, we compared the result of our method with paper [1] and paper [2]'s VSM results.

In paper [1], a novel VSM method is proposed. Firstly, the vertical-and-horizontal-histogram-based method is used to compensate the background of an incoming image. The method eliminates noise coming from the displacement between an incoming image and a background image that is caused by camera vibration. Then, the speed of the vehicles is measured by analyzing the adjustment image. The principal algorithms of the method are background subtraction (BS) and Hough transform. The camera used in the method is uncalibrated-camera-based camera [1].

In paper [2], a novel speed measurement method by tracking the moving vehicles is illustrated. A novel adaptive threshold method is proposed to binaries the outputs from the interframe difference (IFD) and the background subtraction (BS) techniques. The binary outputs are used to detect moving vehicles by the shrinking algorithm. Then, the detected moving vehicles are tracked to estimate their speeds. The principal algorithms of the method are background subtraction (BS), interframe difference (IFD) and shrinking algorithm. The camera used in the method is a calibrated camera [2].

Table 3 presents the average error in different velocity range by the three methods, respectively. From the table, it shows that the method proposed in the paper has a satisfactory performance in different velocity range.

In addition, the stated method can be used to count vehicles. As the camera is fixed on a bridge, and the height of bridge is not high. Also, the processing time of each frame is 25 ms by the proposed method. So, when the vehicles pass the ROI, the time interval between two vehicles in the same lane is long enough to separate them, and the number of the interval can be used as the number of the vehicles passed the lane. Test results show that the detected rate

is up to 99% by the proposed method. But when a big vehicle and a small vehicle pass the ROI at the same time at the double-lane, and the distance between the two vehicles is short, the detected result may be fault.

4. Conclusion

The VSM method on the base of the improved three-frame difference and the proposed gray constraint optical flow algorithm has the characteristics of low cost, low computation and accurate speed measurement. In the method, the contour of moving vehicles can be detected accurate by the improved frame difference algorithm, and the vehicle contour's optical flow value, which is the speed (pixels/s) of the vehicle in the image, is calculated by the proposed gray constraint optical flow algorithm. In the image, we draw the region of interest and only compute the speed of moving target's contour in the region, which can reduce the computational further. By the corresponding ratio between the image pixels and the width of the road, the speed (km/h) of the moving target is calculated. Experiments show that the method is easy to implement and has good robustness. Also, the speed estimate is satisfied. For the three-lane, four-lane and multi-lane's speed measurements, we can improve the detection method to reduce the computation to meet the real-time requirement, and establish the accurate model between the pixels in the image and the width of the road, which will be our next study.

Acknowledgments

This work is supported by National Natural Science Foundation (Grant No. 61174181), Beijing Natural Science Foundation (Grant No. 4102038), China Basic Research (Grant No. 2220132013) and Fundamental Research Funds for the Central Universities (FRF-SD-12-017A).

References

[1] T.T. Nguyen, X.D. Pham, J.H. Song, Compensating background for noise due to camera vibration in uncalibrated-camera-based vehicle speed measurement system, IEEE Trans. Veh. Technol. 60 (January (1)) (2011) 30–43.
[2] T. Celik, H. Kusetogullari, Solar-powered automated road surveillance system for speed violation detection, IEEE Trans. Ind. Electron. 57 (9) (2010) 3216–3227.
[3] Y.-K. Ki, D.-K. Baik, Model for accurate speed measurement using double-loop detectors, IEEE Trans. Veh. Technol. 55 (4) (2006) 1094–1101.
[4] H. Cheng, B. Shaw, J. Palen, B. Lin, B. Chen, Z. Wang, Development and field test of a laser-based nonintrusive detection system for identification of vehicles on the highway, IEEE Trans. Intell. Transp. Syst. 16 (June (2)) (2005) 147–155.
[5] T.X. Mei, H. Li, Measurement of absolute vehicle speed with a simplified inverse model, IEEE Trans. Veh. Technol. 59 (3) (2010) 1164–1171.
[6] L.-D. Damien, G. Christophe, Doppler-based ground speed sensor fusion and slip control for a wheeled rover, IEEE Trans. Mech. 14 (August (4)) (2009) 484–492.
[7] A. Fernández-Caballero, F.J. Gómez, J. López-López, Road-traffic monitoring by knowledge-driven static and dynamic image analysis, Expert Syst. Appl. 35 (October (3)) (2008) 701–719.
[8] Y. Li, L. Yin, Y. Jia, Vehicle speed measurement based on video images, in: 2008 3rd International Conference on Innovative Computing Information and Control (ICICIC), June 2008, p. 439.
[9] R. Canals, A. Roussel, J.-L. Famechon, S. Treuillet, A biprocessor-oriented vision-based target tracking system, IEEE Trans. Ind. Electron. 49 (April (2)) (2002) 500–506.
[10] R. Cucchiara, C. Grana, M. Piccardi, A. Prati, Detecting moving objects, ghosts, and shadows in video streams, IEEE Trans. Pattern Anal. Mach. Intell. 25 (October (10)) (2003) 1337–1342.
[11] T. Schoepflin, D. Dailey, Dynamic camera calibration of roadside traffic management cameras for vehicle speed estimation, IEEE Trans. Intell. Transp. Syst. 4 (June (2)) (2003) 90–98.
[12] Z.-D. Zhang, C.-w. Zhang, Method to improve the accuracy of video-based vehicle speed measurement, J. Shanghai Jiaotong Univ. 44 (10) (2010) 1439–1443.
[13] B.L. Tseng, C.-Y. Lin, J.R. Smith, Real-time video surveillance for traffic monitoring using virtual line analysis, in: IEEE International Conference on Multimedia and Expo, August 2002, pp. 541–544.
[14] J. Wu, Z. Yang, J. Wu, A. Liu, Virtual line group based video vehicle detection algorithm utilizing both luminance and chrominance, in: IEEE Conference on Industrial Electronics and Applications, May 2007, pp. 2854–2858.
[15] T.N. Schoepflin, D.J. Dailey, Algorithms for calibrating roadside traffic cameras and estimating mean vehicle speed, in: IEEE International Conference on Intelligent Transportation Systems, 2007, pp. 277–283.
[16] M. Weng, G. Huang, X. Da, A new interframe difference algorithm for moving target detection, in: Proceedings of International Congress on Image and Signal Processing, October 2010, pp. 285–289.
[17] A. Lookingbill, J. Rogers, D. Lieb, J. Curry, et al., Reverse optical flow for self-supervised adaptive autonomous robot navigation, Int. J. Comput. Vis. 74 (3) (2007) 287–302.
[18] Y. Dong, Video Motion Detection Based on Optical Flow Field, Department of Information Science and Engineering, Shandong University, 2008, M.E. Dissertation.
[19] B.K.P. Horn, B.G. Schunck, Determining optical flow, Artif. Intell. 17 (1981) 185–203.
[20] G. Garibotto, P. Castello, E.D. Ninno, P. Pedrazzi, G. Zan, Speed vision: speed measurement by license plate reading and tracking, in: Proceedings of IEEE International Conference on Intelligent Transportation Systems, 2001, pp. 585–590.
[21] X.C. He, N.H.C. Yung, A novel algorithm for estimating vehicle speed from two consecutive images, in: Proceedings of IEEE Workshop on Applications of Computer Vision, 2007, pp. 12–18.
[22] D.J. Dailey, F.W. Cathey, S. Pumrin, An algorithm to estimate mean traffic speed using uncalibrated cameras, IEEE Trans. Intell. Transp. Syst. 1 (June (2)) (2000) 98–107.
[23] F.W. Cathey, D.J. Dailey, A novel technique to dynamically measure vehicle speed using uncalibrated roadway cameras, in: Proc. IEEE Symp. Intell. Veh., June 2005, pp. 777–782.
[24] L. Grammatikopoulos, G.E. Karras, E. Petsa, Automatic estimation of vehicle speed from uncalibrated video sequences, in: Proc. Int. Symp. Mod. Technol., November 2005, pp. 332–338.
[25] C. Maduro, K. Batista, P. Peixoto, J. Batista, Estimation of vehicle velocity and traffic intensity using rectified images, in: Proceedings of IEEE International Conference on Image Processing, October 2008, pp. 777–780.